Photoprogramming Allostery in Human Serum Albumin

Rindia M. Putri,[†,#,§,⊥] Habiburrahman Zulfikri,[‡,§] Jean Wilfried Fredy,[†] Alberto Juan,[#] Pichayut Tananchayakul,[†] Jeroen J. L. M. Cornelissen,[#] Melissa S. T. Koay,[#] Claudia Filippi,*[,‡] and Nathalie Katsonis*[,†]

[†]Bio-inspired and Smart Materials, MESA+ Institute for Nanotechnology, University of Twente, PO Box 217, 7500 AE Enschede, The Netherlands

[‡]MESA+ Institute for Nanotechnology, University of Twente, 7500 AE Enschede, The Netherlands

[#]Laboratory for Biomolecular Nanotechnology, MESA+ Institute for Nanotechnology, University of Twente, 7500 AE Enschede, The Netherlands

S *Supporting Information*

ABSTRACT: Developing strategies to interfere with allosteric interactions in proteins not only promises to deepen our understanding of vital cellular processes but also allows their regulation using external triggers. Light is particularly attractive as a trigger being spatiotemporally selective and compatible with the physiological environment. Here, we engineered a hybrid protein in which irradiation with light opens a new allosteric communication route that is not inherent to the natural system. We select human serum albumin, a promiscuous protein responsible for transporting a variety of ligands in plasma, and show that by covalently incorporating a synthetic photoswitch to subdomain IA we achieve optical control of the ligand binding in subdomain IB. Molecular dynamics simulations confirm the allosteric nature of the interactions between IA and IB in the engineered protein. Specifically, upon illumination, photoconversion of the switch is found to correlate with a less-coordinated motion of the two subdomains and an increased flexibility of the binding pocket in subdomain IB, whose fluctuations are cooperatively enhanced by the presence of ligands, ultimately facilitating their release. Our combined experimental and computational work demonstrates how harnessing artificial molecular switches enables photoprogramming the allosteric regulation of binding activities in such a prominent protein.
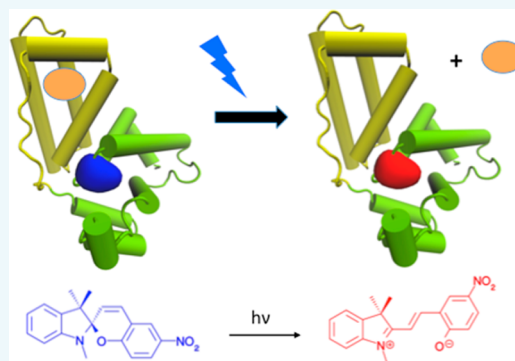
■ INTRODUCTION

In proteins with multiple binding pockets, binding of a ligand at one site often influences the binding of ligands to other remote binding sites, a process also known as allostery.[1−5] Allosteric regulation of protein activity is central to many biological processes; however, the molecular mechanisms by which proteins undergo allosteric regulation remain largely unknown, and allosteric ligand binding has already revealed a number of paradoxes. For example, tightly packed, fully folded proteins can display remarkable structural plasticity dictated by allosteric communication among binding pockets. On the other hand, a structural change in the protein backbone is not always necessary for the binding sites to communicate with each other.[4]

Overall, evidence is growing that allostery is facilitated in dynamic proteins and is often not simply a shape change-induced phenomenon as understood in earlier years[6] but rather is a statistical process in an ensemble of conformational states of the ligand-protein system.[1−4] Pioneering work has also highlighted the limitations of deducing mechanisms from the static equilibrium structures of the end states alone.[1,3]

The state of the art thus calls for tools to manipulate, investigate, and eventually harness the dynamics of allosteric

systems. A recent study reports on the use of temperature and pH control to increase the local conformational entropy of fused proteins that communicate through allostery.[7] A parallel effort toward allosteric engineering consists of implementing allosteric behavior in wholly synthetic biomimetic systems to control ligand binding and catalysis.[8,9] However, previous approaches lack selectivity in space and time, which is a limitation for protein systems operating under physiological conditions, because environmental changes, for instance, in pH or temperature, can lead to unfolding and loss of activity.

In contrast, light offers high spatiotemporal control while being potentially nondestructive toward proteins and applicable under physiological conditions.[10−14] Arguably, the most straightforward strategy to make proteins light-switchable is to make use of artificial molecular photoswitches provided that the stability and the photoswitching properties of the molecular switches are preserved in the protein environment.[15] Light-modulated proteins have been developed to control biological activities, such as directing the secondary structures

of peptides/proteins,[16,17] enzymatic catalysis,[18,19] protein–ligand binding,[20,21] and modulation of protein channels[22,23] and receptors in neural networks.[24] Recently, the emergence of photoswitchable allosteric modulators[25−27] as well as light-activated allosteric channel and DNA-binding protein[28,29] marks a new era of combining allosteric regulation with tailored optical control by incorporation either light-activated protein segments or of synthetic molecular switches.

The human serum albumin (HSA) protein constitutes an ideal playground to design novel optical strategies[30−32] and to modulate specific binding activities. HSA is the most abundant protein in human blood plasma and is the main carrier of a variety of compounds, being able to bind over 120 types of ligands despite its relatively simple monomeric structure.[33] This small protein (66 kDa) is dominated by α-helices and loops and characterized by multiple binding sites (3 primarily for ligands and 7 for fatty acids), which account for its remarkable ability to bind a broad range of compounds.[33,34] This promiscuity offers an opportunity to potentially modulate a large number of binding events, but it is also associated with a challenge as the global structural organization of the binding sites in HSA is very flexible, also adapting to the binding of compounds[35] and enabling multiple binding sites to be coupled through allosteric interactions.[33] Recent investigations by ultrafast time-resolved spectroscopy suggest that these interactions are also associated with ballistic energy flow through the connecting helical structures of HSA.[36]

Here, we create a photoswitchable HSA protein by attaching a photoswitch at subdomain IA covalently and achieve optical control on ligand release at the distinct binding site of subdomain IB. The effect of photoswitching is therefore propagated between two neighboring subdomains that are covalently connected only through a long flexible coil and do not share any helices. The experimental evidence is supported by extensive molecular dynamics (MD) simulations, which rule out any possibility of direct interaction between the photoswitch and the binding site of subdomain IB and reveal that the IB pocket becomes significantly more flexible after photoswitching. In contrast, no enhanced plasticity of subdomain IA is observed, but there is a reduced coordination in the motion of the two subdomains. This dynamic change correlates to a loss of specific interactions of the ligand with the IB pocket and ultimately to the photoinduced release observed experimentally. To the best of our knowledge, allosteric communications between the IA and IB sites have not been reported before. Furthermore, in the absence of the switch, no ligand release is observed upon irradiation. Our experimental study, combined with MD simulations, therefore suggest that it is possible to leverage the dynamic nature of allostery and "wire" a communication pathway that is not intrinsic to the natural system to control the specific binding activity of a protein.

■ RESULTS AND DISCUSSION

Design and Synthesis of a Photoswitchable Albumin Hybrid. We connect a spiropyran photoswitch (SP) to the subdomain IA site covalently by modifying the single surface-accessible free cysteine (Cys34) present in the native structure[37] (Figure 1a). HSA consists of 17 pairs of disulfide linkages that maintain its folded tertiary structure, leaving a single cysteine located at binding site IA (i.e., Cys34) available for chemical modifications.[37] The Michael addition of the thiol of the cysteine to the maleimide moiety of the photoswitch generates a pair of diastereoisomers. However, these
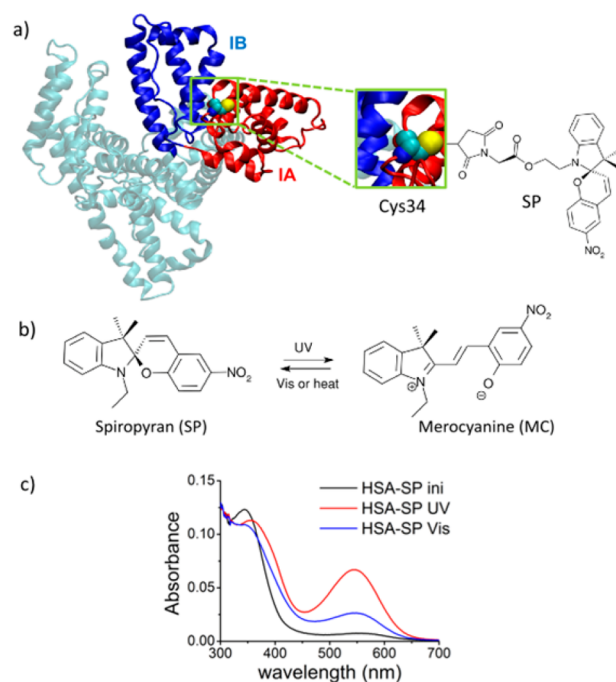

Figure 1. Design and synthesis of a photoswitchable hybrid of human serum albumin (HSA). (a) A spiropyran molecule (SP) is connected covalently to HSA via Cys34 (green) in Tris-HCl buffer pH 7.5 (containing 20% DMSO). The IA and IB subdomains of HSA are shown in red and blue, respectively. (b) Under irradiation with UV light, SP converts to its isomer merocyanine (MC). (c) UV−visible spectra of the hybrid system before (black) and after irradiation with UV light (red) and visible light (blue).

diasteroisomers were not considered independently in our study as we observed no significant difference in their behavior. Moreover, we verified computationally that this diastereoisomery is not determined with regards to the interaction of the photoswitch with the IB pocket. Modification of this cysteine is anticipated to allow selective photoswitching without disrupting the entire protein structure because only one single residue is modified. Moreover, previous experimental studies have suggested that Cys34 is involved in the allosteric regulation of HSA specifically linked to Lys525, although the associated mechanism remains largely unknown.[34] The binding site of HSA examined in this study is located in subdomain IB (residue numbers 108−197), a separate entity that is adjacent to the engineered IA site (residue numbers 4−107).[34] The modification site of Cys34 is 1.3−2.2 nm away from the examined IB binding site (distance relative to binding residues of IB: Lys137, Arg186, Arg117).

Spiropyran is chosen as a photoswitch because, under irradiation with light, it is converted to its open, zwitterionic form, the merocyanine (MC), which is expected to substantially modify electrostatic interactions locally (Figure 1b).[12] In the conditions chosen for this experiment, the conversion of SP to MC is partially reversible upon irradiation with visible light (Figure 1b). The hybrid protein HSA−SP is prepared at room temperature by coupling the free cysteine of HSA to a nitro-spiropyran bearing a maleimide function (Figure S1) via Michael addition in a Tris-HCl buffer (pH 7.5) that also contains 20% dimethylsulfoxide (DMSO) as an organic solvent to solubilize the photoswitch. The nitro group ensures the solubility of the photoswitch in an aqueous environment, in particular of the MC form, by stabilizing the
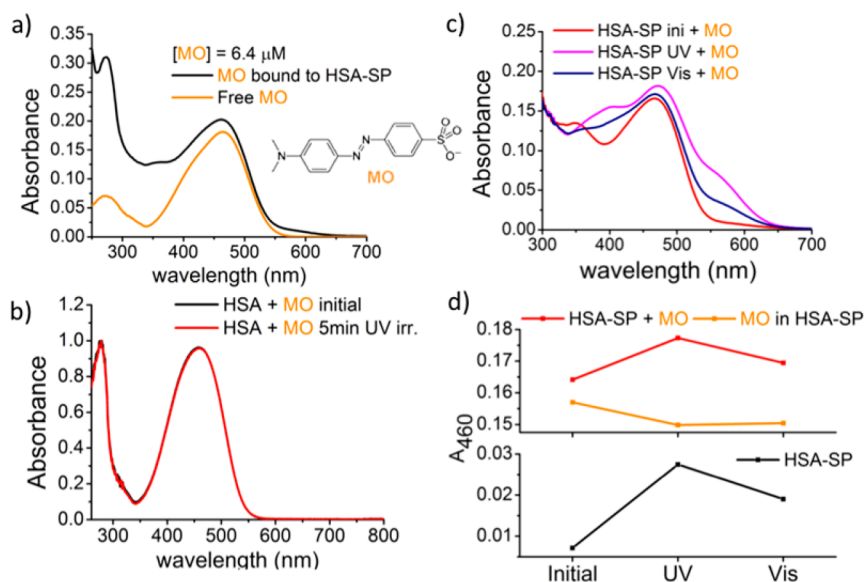
Figure 2. Photoresponsive binding of methyl orange (MO) to subdomain IB. All ligand release and rebinding experiments were repeated three times in situ in Tris-HCl buffer pH 7.5. (a) MO absorption spectra display a positive shift in the visible region when bound to HSA−SP (black) compared to the free dye (orange). (b) Spectra of HSA-bound MO (in the absence of SP) before (black) and after (red) UV irradiation. (c) Photoswitching of HSA−SP with bound MO characterized with UV−visible spectroscopy before (red) and after UV (pink) and Vis (blue) light irradiation. The ligand binding does not hinder the reversible conversion of SP to MC. (d) Optical response of HSA−SP-bound MO (orange) monitored at λ = 460 nm.

phenoxide. It is important to work at pH 7.5 as SP can be spontaneously converted to protonated MC in an acidic environment, which is characterized by strong absorption at λ = 420 nm.[12] Basic conditions also need to be avoided due to the risk of alkaline hydrolysis of the maleimide.[38]

The presence of SP is indicated by its characteristic absorption with λ_{max} = 350 nm at pH 7.5. Furthermore, coelution of both SP (absorption at λ = 350 nm) and HSA (absorption at λ = 280 nm) around V = 16 mL by size-exclusion chromatography indicates that the photoswitch and the protein are coupled covalently (Figure S2a). We confirm that SP remains in its closed, nonprotonated form after covalent attachment to HSA based on the minimal absorption at λ = 420 nm, which indicates the absence of protonated MC (Figure S2b). We deduce that the coupling is quantitatively 1:1 based on the absorption values at λ = 280 and 350 nm (Figure S2b). Prolonging the reaction time from 1 h up to 24 h does not have any effect on the coupling ratio.

Irradiating this albumin hybrid with UV light (λ = 365 nm, 5 min) triggers the appearance of an absorption band at λ_{max} = 550 nm, which signals the transformation of the colorless SP into the colored MC isomer and demonstrates that the photochromic properties of the switch are preserved after its covalent attachment to the protein (Figure 1c). NMR spectroscopy allows us to determine that the degree of photoconversion from SP to MC is ∼40% under our experimental conditions (Figure S2c), suggesting that a mixture of HSA−SP and HSA−MC is present in the photostationary state. Prolonged irradiation, however, is not recommended as the generated heat can disrupt the protein structure and even lead to partial aggregation.[39] Furthermore, upon irradiation with visible light ($\lambda \geq$ 420 nm, 5 min), the band at λ_{max} = 550 nm gradually decreases, indicating that some of the MC form switches back to the colorless SP form. UV−visible spectra reveal that this transformation is not fully reversible (Figure 1c), probably due to the fact that spiropyran

also displays a weak absorption at $\lambda \geq$ 420 nm. This moderate back-conversion in the stationary state is in agreement with the fact that the MC form is known to be favored and stabilized in a polar environment.[12]

We also analyze the effect of irradiation on the global structure of HSA−SP in terms of conformation and hydrodynamic size. Circular dichroism (CD) spectra in phosphate buffer (pH 7.5) confirm that the HSA primarily consists of alpha helical and coiled segments (Figure S 2d). Nevertheless, the CD spectra indicate a small decrease (∼2.9%) in the alpha helical content upon irradiation (Figure S2d, a decrease in the negative CD signal at around 217−228 nm). This decrease is likely associated with possible conformational changes occurring in the vicinity of Cys34 as a result of SP to MC photoconversion. The hydrodynamic size analysis (Figure S2e) does not reveal any significant structural perturbation after irradiation either, confirming that the overall structure of the HSA hybrid remains intact under the conditions of the experiment.

Optical Control over Ligand Binding to Subdomain IB. We examine the behavior of the albumin hybrid before and after irradiation with UV light (λ = 365 nm) with respect to the binding of methyl orange (MO) dye. Methyl orange is known to bind primarily to subdomain IB[40] with an association constants of 2.3×10^5 and 4.8×10^5 M^{-1} for the binding of the first and second ligand, respectively.[41] The binding of dyes to native HSA is associated with characteristic changes in their UV−visible spectra,[41,42] which, for example, have been exploited to determine the concentration of albumin in blood serum.[43] Here, we monitor spectral changes by UV−visible spectroscopy to follow the binding/release of the ligand (Figure 2). For all experiments, an excess of MO ligand (∼4-equivalent) is added to HSA−SP (3.7 μM), and before each spectrum is measured, the unbound MO is removed by spin-filtration. We exclude the possibility that this procedure modifies the equilibrium significantly in light of the large values

of association constants that characterize the binding of ligands to HSA (typically larger than 10^4 M^{-1}). Furthermore, the optical signature of the material is not appreciably modified by spin-filtration (Figure S2b). Finally, by comparing the UV−vis spectra before and after ligand binding, we estimate that the concentration of bound MO is 4.7 μM (protein/ligand ratio is 1:1.3).

At a fixed concentration of ligand, the absorption of free MO in the visible region (λ_{max} = 460 nm) is lower than that of MO bound to HSA−SP (Figure 2a). Importantly, in the absence of spiropyran, we observe that UV irradiation of the ligand−HSA complex does not yield any significant spectral change (Figure 2b). This experiment indicates that MO is stable and not responsive to UV light for our experimental conditions, so any spectral modification upon irradiation is primarily associated with release/binding events.

The binding of MO to the HSA−SP hybrid does not affect the photochromic properties of the photoswitch as verified by UV−visible spectroscopy (Figure 2c). Further examination of the spectral contributions of MO shows a decrease of absorption at λ = 460 nm after 5 min irradiation with UV light (Figure 2d, orange line). The difference can be attributed to the release of MO from subdomain IB. The decrease in the absorption band reveals that ~(16 ± 2)% of the bound MO ligand is released upon UV irradiation (Figure 2d and Figure S3). Reversibility is moderate because only ~(8 ± 1)% of the released MO binds back after subsequent irradiation with visible light for 5 min (Figure 2d and Figure S3). The lack of full reversibility in the binding event is associated with the fact that the molecular switching itself is not reversible fully under the conditions of the experiment. Moreover, before illumination there is an excess of ligand present in solution, whereas after one illumination cycle, the excess ligand has been removed and the equilibrium is likely shifted toward dissociation.

The photoinduced release of the dye from subdomain IB is further corroborated by measuring diffusion before and after irradiation using pulsed-field gradient spin−echo NMR experiments. The diffusion constant of MO in the HSA−MO complex increases from (4.11 ± 0.02) × 10^{-10} m^2/s to (4.28 ± 0.02) × 10^{-10} m^2/s before and after irradiation, respectively. This light-induced increase confirms qualitatively the occurrence of ligand release because free dyes are expected to diffuse faster than the average of protein-bound dyes. For comparison, the diffusion constant of MO is (4.67 ± 0.02) × 10^{-10} m^2/s in the absence of HSA in solution and measured under the same conditions.

Next, to demonstrate that our approach is not limited to one ligand only, we perform photoinduced allosteric experiments with bromocresol green (BG), another dye that binds primarily to subdomain IB (Figure S4).[40] The binding of bromocresol green to HSA results in changes in the absorption spectrum that are similar to those observed for methyl orange (Figure S4a). In native HSA and thus in the absence of spiropyran, no photoinduced spectral changes are observed for the HSA−BG complex (Figure S4b), which demonstrates that bromocresol green is stable against irradiation. In the hybrid system, the binding of BG does not interfere with the photochromic properties of the spiropyran (Figure S4c). Upon irradiation, an increase in absorption is observed at λ = 615 nm (Figure S4d, blue line), which signals release of bound BG upon conversion of SP to MC. On the basis of a similar analysis to the MO case, ~(4.5 ± 0.5)% of bound BG is released upon photoconversion

of spiropyran (Figures S3 and S4d). The lower percentage of released BG is likely related to its binding affinity to HSA, which is 7-fold higher than the binding affinity of MO to HSA.[41,44] Upon subsequent irradiation with visible light (λ ≥ 420 nm), ~(89 ± 11)% of the released ligand rebinds the protein during MC to SP conversion (Figures S3 and S4d), which means that BG displays a higher degree of reversibility than MO. The different degrees of reversibility likely originate from the higher binding constant of BG with subdomain IB of the albumin compared to the binding of MO with the same protein.

To further investigate the release of MO from the IB pocket, we proceed to determine the binding affinity of MO to the engineered HSA by following the fluorescence of tryptophan that is quenched upon binding of MO to the IB pocket (Figure 3a, excitation at λ = 279 nm and emission at λ = 340 nm).
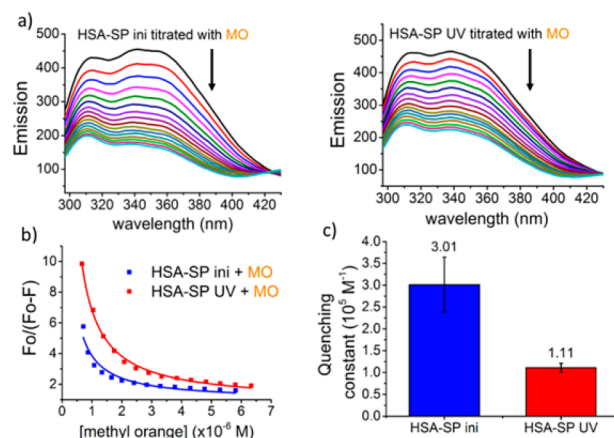

Figure 3. Binding of the methyl orange (MO) ligand to HSA−SP estimated based on Trp fluorescence quenching. (a) Fluorescence emission of HSA−SP titrated with MO without any irradiation (left) and upon irradiation with UV light (right) (excitation at λ = 279 nm and emission at λ = 297−450 nm). (b) Experimental data and Stern−Volmer fit for Trp fluorescence quenching by MO without (blue) and with (red) UV light irradiation. HSA−SP concentration is 6 μM. (c) Effective quenching constants of MO in the hybrid system without and with UV-light irradiation revealing a 2.7-fold decrease upon irradiation.

Notably, the only tryptophan residue in the entire HSA (Trp214) is located at the connecting helix between subdomains IB and IIA.[34] The observed quenching is therefore attributed to energy transfer phenomenon (FRET) between Trp ($\lambda_{emission}$ = 300−400 nm) and MO ($\lambda_{excitation}$ = 350−550 nm) as the distance between Trp214 and IB binding site (3−4 nm) allows such a mechanism to occur.[45] Through a fit with the Stern−Volmer eq (Figure 3b), the protein−ligand associations in the different systems expressed in their quenching constants are summarized in Figure 3c. The effective quenching constants reveal a 2.7-fold decrease in MO binding upon UV light irradiation.

Nature of the Interaction between HSA and the Photoswitch. We perform docking and atomistic MD simulations to elucidate how the photoswitch interacts with the IB pocket. Our docking simulations reveal that the nitro functional group of the photoswitch attached to HSA (PDB ID: 4K2C) can form a hydrogen bond with the Arg144 or the Lys137 residues, which lie on the B2 helix of the IB pocket (Figure 4a and b). Further inspection of the amino acids
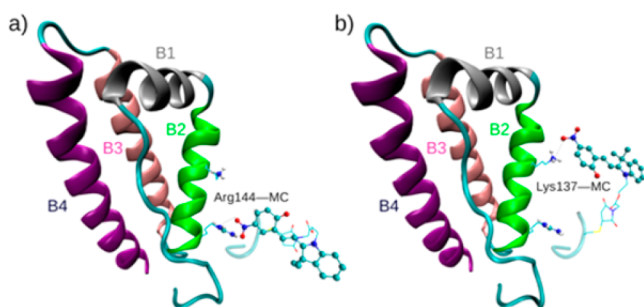
Figure 4. Noncovalent interaction between the photoswitch (MC) and (a) Arg144 and (b) Lys137 side chains of the IB pocket. The pocket consists of a long coil and four α-helices (B1—B4) connected by three short loops.

decorating the triangular gate formed by the coil and the B1 and B2 helices corroborates that these two residues are the only candidates for the formation of a hydrogen bond with the photoswitch.

Starting from different initial configurations of SP and MC hydrogen bonded to Arg144, we observe that the bond is preserved for as long as 100 ns (Figures S6a, b) in some MD simulations. Therefore, even though the reach of SP is shorter by ∼0.1 nm than that of MC (measured by the distance between N_{indole} and N_{nitro}), both switches can form a stable hydrogen bond with this residue. The hydrogen bond of either switch to the somewhat farther and more flexible Lys137 is instead generally weaker and breaks after a few ns of lifting its constraint in the MD simulations (Figure S6c, d). The photoswitch ring then either moves into bulk solvent, interacts with subdomain IA, or is hydrogen bonded to the closer Arg144.

As the phenoxide oxygen (O_{ph}) of MC can act as hydrogen-bond acceptor, we also design two possible configurations where the nitro group strongly perturbs the IB pocket and is held inside by hydrogen bonds (Figure S7a, c). In both cases,

these bonds quickly deteriorate in the MD simulations (Figure S7b, d), and the nitrophenoxide group exits the pocket to interact with bulk solvent. We can therefore exclude a direct interference of the photoswitch with the interior of the IB pocket. On the basis of these findings, we start all MD simulations in the presence of MO with the photoswitch hydrogen bonded to either Arg144 or Lys137. The latter configuration predominantly results again in trajectories where the switch does not interact with the pocket.

Mechanistic Insight on Ligand Release. The IB pocket of native HSA can accommodate up to two MOs,[41] and our CD spectra indicate that this is also true for the hybrid system (section S5). To generate initial configurations for MD simulations, we dock the MO ligand into multiple host coordinates extracted from the MD simulations of the native and hybrid proteins. The many resulting structures can be grouped in three sets depicted in Figure 5a−c. We then dock a second MO ligand in the snapshots extracted from the MD simulations of these HSA:1MO systems. The resulting configurations are combinations of the positions we have identified for a single MO. For instance, two MOs in position A yield the parallel AA configuration (Figure 5d), whereas positions A and B give the antiparallel AB arrangement (Figure 5e). We also find recurrence of the AC and CC configurations (Figure 5f and Figure S8), whereas BB and BC are not observed as they are likely characterized by higher binding energies.

Starting from these docking coordinates, we rarely observe direct ligand release in our extensive MD simulations of the native and hybrid systems. In the 24 simulations (100 ns each) with one MO and 30 simulations (150 ns each) with two MOs, we observe two cases of ligand release, namely in native HSA with (1) one MO in position A, which exits the pocket between the coil and the B4 helix, and (2) two ligands in the AC configuration (Figure 5f), where the MO at position A exits the triangle gate. Importantly, in both cases the release of the MO happens in conjunction with permanent loss of its
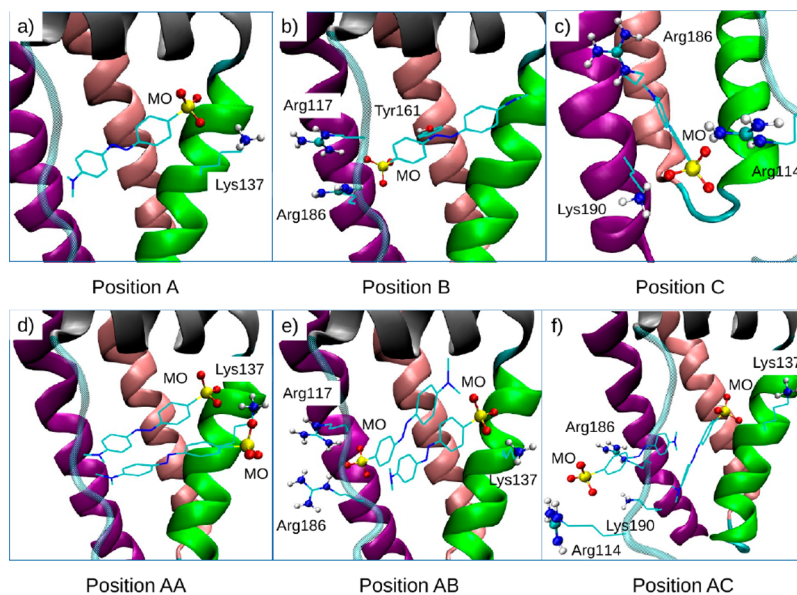

Figure 5. MO configurations in the IB pocket. One ligand: (a) MO is kept by a hydrogen bond between its sulfonate group and Lys137; (b) the sulfonate group of MO forms three hydrogen bonds with Arg117, Arg186, and Tyr138 of different secondary structures; (c) the sulfonate group interacts with Arg114 and Arg117 (not shown) on the coil and Arg186 and Lys190 on the B4 helix. Two ligands: (d) parallel (AA), (e) antiparallel (AB), and (f) cross (AC) configurations where Lys137 stabilizes the A ligand.
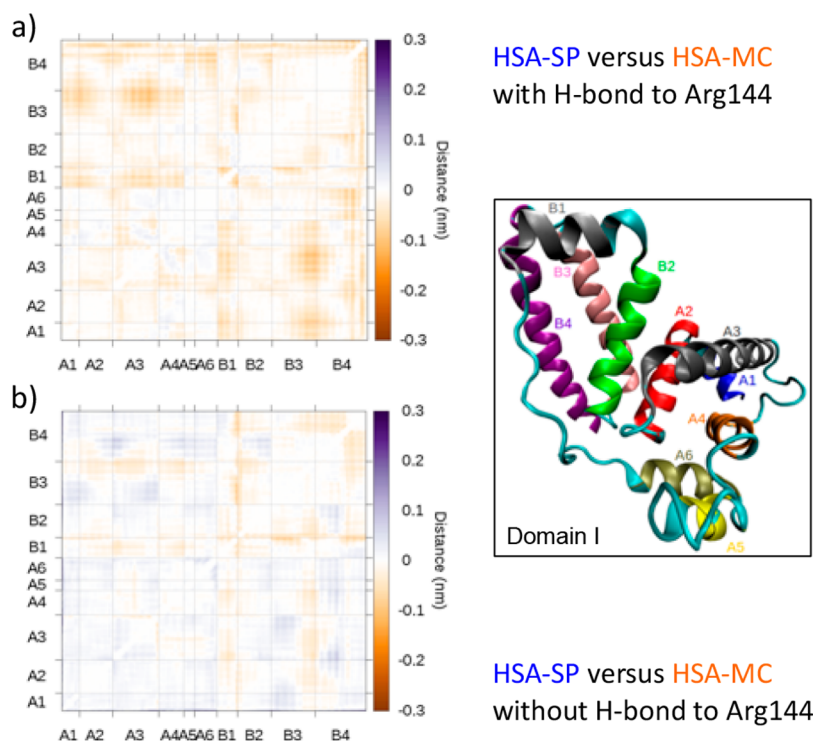
Figure 6. Relative distance fluctuations of domain I of HSA−SP and HSA−MC complexed with two MO ligands in the AB configuration. Areas that are mostly blue correspond to higher fluctuations in the HSA−SP complex, whereas areas that are mostly orange correspond to higher fluctuations in the HSA−MC complex. The fluctuations are depicted for the ten helices of domain I, namely, the A1−A6 and B1−B4 helices of the IA and IB subdomains, respectively, as shown in the inset (right). The change in the relative fluctuation within each subdomain is visible in the A1−A6 and the B1−B4 diagonal corners, whereas the variation in the cross-fluctuation between IA and IB is shown in the (A1−A6, B1−B4) off-diagonal corners. (a, b) The IB pocket is more flexible upon photoswitching (dominant orange area in the B1−B4 corner). In (a), the enhanced cross-fluctuations upon photoswitching are observed in the presence of a hydrogen bond of the switch to Arg144 as indicated by the dominant orange area in the (A1−A6, B1−B4) off-diagonal corners.

hydrogen bond with Lys137 (Figures S9 and S10), which maintains the ligand at position A. Of the possible MO configurations, the A position is in fact the least stable, having only one hydrogen bond with the binding pocket. We note that one should instead not ascribe particular significance to the absence of release in most of our simulations: the protein binds and dissociates the ligand dynamically, a phenomenon that can occur over very different time scales. For direct comparison with the experimentally determined percentage of ligand release, MD simulations would have to be performed over seconds or even minutes, and these time scales are currently not accessible computationally.

Given the role of the MO-Lys137 hydrogen bond in stabilizing the ligand at position A, we probe its relative occurrence in the native and hybrid systems. We focus the analysis on the 2MO complexes (more abundant than the 1MO ones under our experimental conditions: protein/ligand ratio = 1:1.3)[41] in the AB arrangement. Among the three configurations with a MO-Lys137 bond, AB is in fact the most stable and, consequently, the most abundant thermodynamically: the two MOs can form in total three hydrogen bonds with the IB pocket (Figure 5e), are π-stacked, and minimize the repulsion between the negatively charged sulfonate groups. In our MD simulations with two AB MOs, we find that the occurrence of the MO-Lys137 hydrogen bond is greater than 90% in native HSA (Figure S11 and Table S1) but is reduced to maximums of 63 and 17% in the presence of SP and MC, respectively. In the HSA−SP simulations, the presence of a hydrogen bond between SP and Arg144 seems to help preserve

the MO-Lys137 bond, whose occurrence increases from 1 to 63% when the SP−Arg144 bond is formed. In the HSA−MC complex, this additional interaction between the IA and IB subdomains via Arg144 has the opposite effect, leading to a decrease in the occurrence of the MO-Lys137 bond from a maximum of 17 to 3%. Overall, these findings indicate that switching spiropyran destabilizes the MO-Lys137 bond (see also section S10) and consequently facilitates ligand release.

Next, we investigate how the switch affects the coupling and the internal flexibility of the binding IB pocket and the IA subdomain (where the switch is attached) by computing the fluctuations of the Cα−Cα distances between different amino acids in our MD trajectories. High fluctuations within IB indicate a greater propensity for ligand dissociation, and high cross-fluctuations between IA and IB signal a reduced coordination in their relative motion, which can in turn enhance the overall mobility of the IB pocket and further ease ligand release. The relative fluctuations of the HSA−SP and HSA−MC complexed with two MO ligands in the AB configuration are shown in the presence and absence of a hydrogen bond between the switch and Arg144 in Figure 6a and b, respectively. In both cases, upon switching, the IB pocket becomes more flexible with the B1 helix being the most fluctuating α-helix in the subdomain. Although the presence of MC in this complex appears to be sufficient to increase the flexibility of subdomain IB with respect to the SP case, we find that the additional hydrogen bond to Arg144 enhances the flexibility of all regions and causes the largest changes in the cross-fluctuations of the two subdomains (Figure 6a as

compared to Figure 6b). This bond has in fact an opposite effect on the HSA−SP/HSA−MC system, increasing/decreasing the overall rigidity of domain I (Figure S12) and, consequently, the stability of the ligand in the pocket as also found before in relation to the occurrence of the MO-Lys137 bond. Furthermore, we analyze the role of the MO ligands in stabilizing the IB pocket in the native and hybrid systems. Whereas the presence of the ligands in HSA and HSA−SP reduces the fluctuations of the binding pocket (Figure S13a−c) as also observed in other protein−ligand systems, it has the opposite effect in HSA−MC, where it enhances the flexibility of the pocket (Figure S13d, e), particularly in the presence of the MC-Arg144 hydrogen bond. All factors therefore concur to facilitate ligand release upon photoswitching.

Finally, we briefly analyze the parallel AA configuration of the two ligands (Figure 5d) as regards the stability of the MO-Lys137 hydrogen bond and the internal dynamics of the protein complex. In this arrangement, both negatively charged sulfonate groups of the MOs point toward bulk solvent, and their interaction is mediated by the positively charged Lys137, which helps overcome their strong electrostatic repulsion by forming a salt bridge. In our MD simulations, we find however that this salt bridge varies in occurrence and is not well positioned. Even in native HSA (Figure S14 and Tables S2 and S3), this is responsible for a lower occurrence of the MO-Lys137 hydrogen bond as well as higher fluctuations of the whole domain I (Figure S15). Upon switching from SP to MC, the IB pocket increases its fluctuations (Figure S16). Moreover, as in the AB configuration, the motions of the IA and IB subdomains become less coordinated, particularly in the presence of a hydrogen bond between the switch and Arg144. Also for the AA configuration, our findings support a mechanism through which the IB pocket becomes more flexible after photoswitching of the spiropyran, which in turn facilitates release of the ligands. Notably, molecular dynamics confirm that the covalent incorporation of the photoswitch and the subsequent photoswitching event do not alter the protein backbone significantly (Figures S17−S20); upon illumination, only a minor change is observed in the CD spectrum (Figure S2d), which we associate to the modified site only (Table S4).

CONCLUSIONS

We have engineered a photoresponsive hybrid of human serum albumin in which irradiation results in ligand release through allosteric communication between subdomains IA and IB while preserving the overall structure of the protein. Although the decrease in the ligand binding affinity is at most up to 3-fold, a significant impact can still be expected as albumin is involved in complex cellular networks. A similar magnitude (4-fold decrease) of photocontrolled binding affinity has in fact been shown to affect the functionality of the catabolite activator protein.[10,20] Our findings are therefore especially relevant in light of HSA being a promiscuous protein that binds a very large number of ligands contrarily to the catabolite activator protein that is known to bind only to DNA and ATP derivatives.

Molecular dynamics simulations indicate that the covalent attachment of the switch at IA reduces the stability of ligand binding to a key residue of the IB pocket, especially after photoconversion of the spiropyran switch to merocyanine. Switching correlates with an increased flexibility of the IB pocket and a less coordinated motion of the two subdomains, which further facilitates ligand release. Furthermore, the

presence of the ligands acts cooperatively to enhance the fluctuations of the binding pocket.

Allosteric communications between the IB and IA subdomains of albumin are unprecedented. The remote control of a binding pocket by switching at a neighboring site opens new opportunities for preprogramming and photocontrolling allosteric regulation externally as well as inducing new channels of allosteric interaction in human serum albumin. We envision that similar engineering strategies could be extended to systems with higher-order structures and further on to supramolecular protein-based hybrids.[46]

EXPERIMENTAL SECTION

Materials. The human serum albumin (HSA) was purchased from Sigma-Aldrich. All experiments were performed at pH 7.5 in a Tris-HCl buffer (containing 150 mM NH4Cl). Chemicals were purchased from Sigma-Aldrich unless stated otherwise.

Synthesis and Characterization of Hybrid System. A 10-fold excess of nitro-spiropyran bearing a maleimide functional group was added to HSA (in 20 mM Tris-HCl buffer pH 7.5 containing 20% DMSO) at room temperature and incubated for an hour. The unbound spiropyran was removed by repeated spin-filtration (Corning Spin-X UF 10k MWCO membrane filters) each for 20 min at 6,000 rpm (Eppendorf centrifuge 5415R) or with size-exclusion chromatography (preparative column Superose 6 10/100 GL, GE Healthcare FPLC Äkta purifier 900 with a 24 mL bed volume). Prior to injecting the samples into the column, all samples were dialyzed against Tris-HCl buffer pH 7.5 to remove the DMSO using 12−14 kDa dialysis membranes (Spectra/Por). The purified hybrid system was further characterized with s UV−visible spectrometer (PerkinElmer Lambda 850).

Molecular Docking Simulations. To generate representative initial configurations of the HSA−SP and HSA−MC systems for our MD simulations, we started from the X-ray coordinates of HSA (PDB entry: 4K2C) and covalently attached the photoswitch using the flexible side chain approach[47] implemented in the Autodock version 4.2 program.[48] We connected one Cα of the maleimide ring to the sulfur atom of Cys34 and allowed all rotatable bonds of both cysteine and the attached photoswitch to vary to minimize the empirical binding energy of the switch to the protein while treating the rest of the protein as a rigid object. Atomic interactions were modeled using the default parameters of AutoDock 4.2. Docking simulations were performed using the Lamarckian Genetic Algorithm. We extended the default search parameters for efficient covalent docking of both modified Cys34 residues, which have nine rotatable single bonds. The number of individuals in the population was increased to 200; the maximum number of energy evaluations carried out during each LGA run was set to 10^7, and 200 poses were requested in each simulation. The resulting poses were clustered with AutoDock with 0.2 nm RMSD tolerance.

The insertion of the MO ligand into the IB pocket was also conducted with the AutoDock program. We employed default parameters for the LGA runs and asked for 50 poses per simulation. MD snapshots of the IB subdomain taken every 100 ps were used as targets for docking one MO ligand to produce the HSA:1MO complexes. The same procedure was also applied to obtain the HSA:2MO from the HSA:1MO trajectories. We collected the poses that correspond to the most stable configuration of ligand(s) in the IB pocket from

each docking result and clustered the compiled frames using the clustering plugin of VMD with 0.2 nm RMSD tolerance after aligning the backbone of the IB subdomain.

Molecular Dynamics Simulations. Atomistic MD simulations were performed with the GROMACS version 4.5 package[49] and the Amber99SB*-ILDN force field[50,51] for the protein. Because the photoswitch is attached covalently to the protein, we constructed its force field to be compatible with the Amber99SB*-ILDN procedure. The force field for the MO molecule is built according to the GAFF recipe.[52] We added the missing nonhydrogen atoms in the X-ray structure of HSA using the WHAT IF program[53] and protonated the amino acid residues compatibly to a pH of 7.5 using the PDB 2PQR server.[54] We then solvated the monomeric form of HSA in a 0.15 M NaCl water solution in a $12 \times 12 \times 12$ nm^3 periodic simulation box. The bonded parameters of the water molecules were constrained with the SETTLE algorithm.[55] The electrostatic and van der Waals interactions were evaluated by employing the particle mesh Ewald (PME) method[56] with a cutoff of 1 nm. The structure of the system was then optimized in a steepest-decent energy minimization to avoid clashes among atoms before running any simulations.

In preparation for each MD run of HSA, HSA−SP, or HSA−MC, the system was first thermally equilibrated to 300 K in an NVT ensemble for 0.5 ns with a velocity-rescaling thermostat[57] with a coupling constant of 0.1 ps. The simulation was then continued in an NPT ensemble for 0.5 ns to reach a stable pressure of 1 atm using a Parrinello−Rahman barostat[58] with a coupling constant of 2 ps while maintaining a temperature of 300 K. The LINCS constraint algorithm[59] was applied to all bonds in the protein to enable the use of a larger time step of 2 fs. In the temperature and pressure equilibration runs, the positions of nonhydrogen atoms in the protein were restrained with a force constant of 1000 kJ mol^{-1} nm^{-2}.

Each production run of the HSA-photoswitch configurations consisted of three consecutive MD simulations in an NPT ensemble for a total of 170 ns at least. First, we ran a 10 ns MD simulation where we restrained the position of the backbone and the hydrogen-bond distance(s) between the photoswitch and protein. Second, we removed the restrain on the backbone in a 40 ns MD simulation to reach a stable conformation that still held the photoswitch-protein hydrogen bond(s). Then, we proceeded with a 120 ns (170 ns for the protein:2MO complexes) simulation without any restraints. For the native HSA simulations, the second step was performed without any restraints. If an MO was present in the IB pocket, the position of its heavy atoms was restrained only in the first step of simulation. Analysis of the MD trajectories was carried out over the last 100 ns (150 ns for the protein:2MO complexes) of the simulations using equidistant MD snapshots taken every 100 ps.

Analysis of Internal Dynamics. The global rigidity/flexibility of the protein in an MD simulation was investigated by computing the fluctuations in the distance of the amino acid residues as

$$f_{ij} = \sqrt{d_{ij} - \overline{d}_{ij}}$$

where d_{ij} is the distance between the Cα atoms of residues i and j and $\overline{d}_{ij}$ is its average. Residues that lie on the coil structure, including the modified Cys34, are omitted in the calculation as they naturally fluctuate in an uncorrelated way.

The square of this quantity is also known in the literature as the coordination propensity (CP).[60] The distance-fluctuation analysis was performed using the CONAN code (https://hits-mbm.github.io/conan).

Analysis of Photoresponsive Ligand Binding. A 4-fold excess of ligand (either methyl orange or bromocresol green) was added to the hybrid system (3.7 μM in 20 mM Tris-HCl buffer pH 7.5) at room temperature and incubated for at least 3 h. The unbound ligand was removed with repeated spin filtration. The samples were irradiated with UV light (λ = 365 nm, bluepoint LED Honle Technology, 40 mW/cm^2) for 5 min and subsequently with visible light ($\lambda \geq 420$ nm, Edmund MI-150 High-intensity Illuminator) for 5 min. The absorption spectra were recorded with PerkinElmer Lambda 850 UV−visible spectrometer. For the fluorescence quenching studies, a 3 mL solution of the hybrid system in 20 mM Tris-HCl buffer at pH 7.5 was placed inside a cuvette with a magnetic stirring system and titrated with the ligand in a microscale addition. After each addition, the solution was incubated and stirred for 3 min. Afterward, the emission spectra at λ = 297−450 nm (excitation at 279 nm) were recorded using a PerkinElmer fluorescence spectrometer. All experiments were reproduced a minimum of three times.

PFGSE-NMR Experiments. All NMR experiments were measured using a Bruker Avance II NMR 600 MHz spectrometer equipped with a triple-nucleus TXI probe head with a z-gradient coil and a Great 3/10 gradient amplifier. All experiments were performed at 300 K using standard pulse sequences from the Bruker library. Pulsed-field gradient spin−echo (PFGSE) NMR experiments were carried out by using the pulse sequence of longitudinal-eddy-current delay (LED) with bipolar gradient pulses with a diffusion delay (Δ) of 0.2 s and gradient length (δ) of 1200 μs and 5 ms of eddy-current delay. The gradient strength was varied from 5 to 95%. A total of 128 transients were collected for each of the 20 increment steps with a recycle delay of 2 s. Pseudo-2D DOSY plots were processed with the standard Bruker software; the diffusion coefficients were determined by the T1/T2 "vargrad" SimFit fitting routine. Calibration of the field gradient strength was achieved by measuring the value of translational diffusion coefficient (D) for the residual ^{1}H signal in D$_2$O (99.99%, ^{2}H atom), $D = 1.91 \times 10^{-9}$ m^2/s.

Determination of Binding Constants. The formation of a protein−ligand complex is associated with static quenching of protein fluorescence by the bound ligand, i.e., we can approximate that the quenching constant is equal to the association constant. The quenching constant is obtained from the modified Stern−Volmer equation

$$\frac{F_o}{\Delta F} = \frac{1}{f_a \cdot K_a \cdot [Q]} + \frac{1}{f_a}$$

where ΔF is the difference in fluorescence emission with and without the quencher Q in the system, Q represents the free quencher, f_a represents the fraction of accessible fluorescence, and K_a is the effective quenching constant.[61,62]

Another technique to determine the binding constants is isothermal microcalorimetry. However, because the MC form can be partially converted back to SP form during the hours of automated measurement, this technique is not applicable here.

Analysis of Global Structure. The conformation of the protein (0.1 μM) before and after irradiation in 10 mM phosphate buffer pH 7.5 was analyzed with a Jasco J-1500

circular dichroism spectrometer. The hydrodynamic size of the protein before and after irradiation in 20 mM Tris-HCl buffer pH 7.5 was determined with dynamic light scattering (Nanotrac Wave, Microtrac).

Data and Schematic Representation. All data plotting and mathematical fitting were performed with OriginPro 9.0 software. For CD spectra, the raw data was smoothed using the Savitzky-Golay filter in OriginPro 9.0 software. Protein structures are rendered using VMD 1.9.2 software, and chemical structures are drawn using ChemBioDraw Ultra 12.0 software.

■ ASSOCIATED CONTENT

Ⓢ Supporting Information

The Supporting Information is available free of charge on the ACS Publications website at DOI: 10.1021/acs.bioconjchem.8b00184.

> Synthesis and characterization of the photoswitch, supporting data for characterization of the HSA−SP hybrid, calibration curves, analysis of bromocresol green binding, and supporting data from molecular dynamics simulations (PDF)

■ AUTHOR INFORMATION

Corresponding Authors
*E-mail: c.filippi@utwente.nl.
*E-mail: n.h.katsonis@utwente.nl.

ORCID Ⓞ
Jeroen J. L. M. Cornelissen: 0000-0002-9728-5043
Claudia Filippi: 0000-0002-2425-6735
Nathalie Katsonis: 0000-0003-1054-6544

Present Address
⊥R.M.P.: Biochemistry Division, Department of Chemistry, Faculty of Mathematics and Natural Sciences, Bandung Institute of Technology, Jl. Ganesha 10 Bandung 40132, Indonesia.

Author Contributions
§R.M.P. and H.Z. contributed equally to this work.

Notes
The authors declare no competing financial interest.

■ ACKNOWLEDGMENTS

■ REFERENCES

(1) Motlagh, H. N., Wrabl, J. O., Li, J., and Hilser, V. J. (2014) The ensemble nature of allostery. *Nature* 508, 331−339.

(2) Fenton, A. W. (2008) Allostery: an illustrated definition for the 'second secret of life'. *Trends Biochem. Sci.* 33, 420−425.

(3) Kern, D., and Zuiderweg, E. R. P. (2003) The role of dynamics in allosteric regulation. *Curr. Opin. Struct. Biol.* 13, 748−757.

(4) Tsai, C.-J., del Sol, A., and Nussinov, R. (2008) Allostery: absence of a change in shape does not imply that allostery is not at play. *J. Mol. Biol.* 378, 1−11.

(5) Ferreon, A. C. M., Ferreon, J. C., Wright, P. E., and Deniz, A. A. (2013) Modulation of allostery by protein intrinsic disorder. *Nature* 498, 390−394.

(6) Changeux, J.-P. (2013) 50 years of allosteric interactions: the twists and turns of the models. *Nat. Rev. Mol. Cell Biol.* 14, 819−829.

(7) Choi, J. H., Laurent, A. H., Hilser, V. J., and Ostermeier, M. (2015) Design of protein switches based on an ensemble model of allostery. *Nat. Commun.* 6, 6968.

(8) Brown, R. A., Diemer, V., Webb, S. J., and Clayden, J. (2013) End-to-end conformational communication through a synthetic purinergic receptor by ligand-induced helicity switching. *Nat. Chem.* 5, 853−860.

(9) Tonga, G. Y., Jeong, Y., Duncan, B., Mizuhara, T., Mout, R., Das, R., Kim, S. T., Yeh, Y.-C., Yan, B., Hou, S., et al. (2015) Supramolecular regulation of bioorthogonal catalysis in cells using nanoparticle-embedded transition metal catalysts. *Nat. Chem.* 7, 597−603.

(10) Szymański, W., Beierle, J. M., Kistemaker, H. A. V., Velema, W. A., and Feringa, B. L. (2013) Reversible photocontrol of biological systems by the incorporation of molecular photoswitches. *Chem. Rev.* 113, 6114−6178.

(11) Beharry, A. A., and Woolley, G. A. (2011) Azobenzene photoswitches for biomolecules. *Chem. Soc. Rev.* 40, 4422−4437.

(12) Klajn, R. (2014) Spiropyran-based dynamic materials. *Chem. Soc. Rev.* 43, 148−184.

(13) Nguyen, D. P., Mahesh, M., Elsässer, S. J., Hancock, S. M., Uttamapinant, C., and Chin, J. W. (2014) Genetic encoding of photocaged cysteine allows photoactivation of TEV protease in live mammalian cells. *J. Am. Chem. Soc.* 136, 2240−2243.

(14) Broichhagen, J., and Trauner, D. (2014) The *in vivo* chemistry of photoswitched tethered ligands. *Curr. Opin. Chem. Biol.* 21, 121−127.

(15) Putri, R. M., Fredy, J. W., Cornelissen, J. J. L. M., Koay, M. S. T., and Katsonis, N. (2016) Labelling bacterial nanocages with photoswitchable fluorophores. *ChemPhysChem* 17, 1815−1818.

(16) Kumita, J. R., Smart, O. S., and Woolley, G. A. (2000) Photocontrol of helix content in a short peptide. *Proc. Natl. Acad. Sci. U. S. A.* 97, 3803−3808.

(17) Woolley, G. A. (2005) Photocontrolling peptide α-helices. *Acc. Chem. Res.* 38, 486−493.

(18) Schierling, B., Noël, A.-J., Wende, W., Hien, L. T., Volkov, E., Kubareva, E., Oretskaya, T., Kokkinidis, M., Römpp, A., Spengler, B., et al. (2010) Controlling the enzymatic activity of a restriction enzyme by light. *Proc. Natl. Acad. Sci. U. S. A.* 107, 1361−1366.

(19) Aizawa, M., Namba, K., and Suzuki, S. (1977) Light-induced enzyme activity changes associated with the photoisomerization of bound spiropyran. *Arch. Biochem. Biophys.* 182, 305−310.

(20) Bose, M., Groff, D., Xie, J., Brustad, E., and Schultz, P. G. (2006) The incorporation of a photoisomerizable amino acid into proteins in *E. coli. J. Am. Chem. Soc.* 128, 388−389.

(21) Woolley, G. A., Jaikaran, A. S. I., Berezovski, M., Calarco, J. P., Krylov, S. N., Smart, O. S., and Kumita, J. R. (2006) Reversible photocontrol of DNA binding by a designed GCN4-bZIP protein. *Biochemistry* 45, 6075−6084.

(22) Koçer, A., Walko, M., Meijberg, W., and Feringa, B. L. (2005) A light-actuated nanovalve derived from a channel protein. *Science* 309, 755−758.

(23) Banghart, M. R., Volgraf, M., and Trauner, D. (2006) Engineering light-gated ion channels. *Biochemistry* 45, 15129−15141.

(24) Tochitsky, I., Banghart, M. R., Mourot, A., Yao, J. Z., Gaub, B., Kramer, R. H., and Trauner, D. (2012) Optochemical control of genetically engineered neuronal nicotinic acetylcholine receptors. *Nat. Chem.* 4, 105−111.

(25) Pittolo, S., Gómez-Santacana, X., Eckelt, K., Rovira, X., Dalton, J., Goudet, C., Pin, J.-P., Llobet, A., Giraldo, J., Llebaria, A., et al. (2014) An allosteric modulator to control endogenous G protein-coupled receptors with light. *Nat. Chem. Biol.* 10, 813−815.

(26) Volgraf, M., Gorostiza, P., Szobota, S., Helix, M. R., Isacoff, E. Y., and Trauner, D. (2007) Reversibly caged glutamate: a photochromic agonist of ionotropic glutamate receptors. *J. Am. Chem. Soc.* 129, 260−261.

(27) Schönberger, M., and Trauner, D. (2014) A photochromic agonist for μ-opioid receptors. *Angew. Chem., Int. Ed. 53*, 3264−3267.

(28) Volgraf, M., Gorostiza, P., Numano, R., Kramer, R. H., Isacoff, E. Y., and Trauner, D. (2006) Allosteric control of an ionotropic glutamate receptor with an optical switch. *Nat. Chem. Biol. 2*, 47−52.

(29) Strickland, D., Moffat, K., and Sosnick, T. R. (2008) Light-activated DNA binding in a designed allosteric protein. *Proc. Natl. Acad. Sci. U. S. A. 105*, 10709−10714.

(30) Rhee, K. W., Gabriel, D. A., and Johnson, C. S., Jr. (1985) Evidence of chemical exchange effects in holographic relaxation spectroscopy: the binding of benzospiropyran to bovine serum albumin. *J. Phys. Chem. 89*, 3193−3195.

(31) Fuentealba, D., Kato, H., Nishijima, M., Fukuhara, G., Mori, T., Inoue, Y., and Bohne, C. (2013) Explaining the highly enantiomeric photocyclodimerization of 2-anthracenecarboxylate bound to human serum albumin using time-resolved anisotropy studies. *J. Am. Chem. Soc. 135*, 203−209.

(32) Kawamura, K., Osawa, K., Watanobe, Y., Saeki, Y., Maruyama, N., and Yokoyama, Y. (2017) Photocyclization of photoswitches with high enantioselectivity in human serum albumin in an artificial environment. *Chem. Commun. 53*, 3181−3184.

(33) Ascenzi, P., and Fasano, M. (2010) Allostery in a monomeric protein: the case of human serum albumin. *Biophys. Chem. 148*, 16−22.

(34) Fanali, G., di Masi, A., Trezza, V., Marino, M., Fasano, M., and Ascenzi, P. (2012) Human serum albumin: from bench to bedside. *Mol. Aspects Med. 33*, 209−290.

(35) Yang, F., Bian, C., Zhu, L., Zhao, G., Huang, Z., and Huang, M. (2007) Effect of human serum albumin on drug metabolism: structural evidence of esterase activity of human serum albumin. *J. Struct. Biol. 157*, 348−355.

(36) Li, G. F., Magana, D., and Dyer, R. B. (2014) Anisotropic energy flow and allosteric ligand binding in albumin. *Nat. Commun. 5*, 3100.

(37) Kratz, F., Warnecke, A., Scheuermann, K., Stockmar, C., Schwab, J., Lazar, P., Drückes, P., Esser, N., Drevs, J., Rognan, D., et al. (2002) Probing the cysteine-34 position of endogenous serum albumin with thiol-binding doxorubicin derivatives. *J. Med. Chem. 45*, 5523−5533.

(38) Khan, M. N. (1984) Kinetics and mechanism of the alkaline hydrolysis of maleimide. *J. Pharm. Sci. 73*, 1767−1771.

(39) Davies, M. J. (2003) Singlet oxygen-mediated damage to proteins and its consequences. *Biochem. Biophys. Res. Commun. 305*, 761−770.

(40) Zsila, F. (2013) Subdomain IB is the third major drug binding region of human serum albumin: toward the three-sites model. *Mol. Pharmaceutics 10*, 1668−1682.

(41) Ambrosetti, R., Bianchini, R., Fisichella, S., Fichera, M., and Zandomeneghi, M. (1996) Resolution of the absorbance and CD spectra and formation constants of the complexes between human serum albumin and methyl orange. *Chem. - Eur. J. 2*, 149−156.

(42) Rodkey, F. L. (1965) Direct spectrophotometric determination of albumin in human serum. *Clin. Chem. 11*, 478−487.

(43) Keyser, J. W. (1961) Rapid estimation of albumin and total protein in small amounts of blood serum. *Clin. Chim. Acta 6*, 445−447.

(44) Trivedu, V. D., Saxena, I., Siddiqui, M. U., and Qasim, M. A. (1997) Interaction of bromocresol green with different serum albumins studied by fluorescence quenching. *IUBMB Life 43*, 1−8.

(45) Ray, P. C., Fan, Z., Crouch, R. A., Sinha, S. S., and Pramanik, A. (2014) Nanoscopic optical rulers beyond the FRET distance limit: fundamentals and applications. *Chem. Soc. Rev. 43*, 6370−6404.

(46) Yang, L., Liu, A., Cao, S., Putri, R. M., Jonkheijm, P., and Cornelissen, J. J. L. M. (2016) Self-assembly of proteins: towards supramolecular materials. *Chem. - Eur. J. 22*, 15570−15582.

(47) Bianco, G., Forli, S., Goodsell, D. S., and Olson, A. J. (2016) Covalent docking using autodock: two-point attractor and flexible side chain methods. *Protein Sci. 25*, 295−301.

(48) Morris, G. M., Huey, R., Lindstrom, W., Sanner, M. F., Belew, R. K., Goodsell, D. S., and Olson, A. J. (2009) AutoDock4 and AutoDockTools4: automated docking with selective receptor flexibility. *J. Comput. Chem. 30*, 2785−2791.

(49) van der Spoel, D., Lindahl, E., Hess, B., Groenhof, G., Mark, A. E., and Berendsen, H. J. C. (2005) GROMACS: fast, flexible, and free. *J. Comput. Chem. 26*, 1701−1718.

(50) Best, R. B., and Hummer, G. (2009) Optimized molecular dynamics force fields applied to the helix−coil transition of polypeptides. *J. Phys. Chem. B 113*, 9004−9015.

(51) Lindorff-Larsen, K., Piana, S., Palmo, K., Maragakis, P., Klepeis, J. L., Dror, R. O., and Shaw, D. E. (2010) Improved side-chain torsion potentials for the amber ff99SB protein force field. *Proteins: Struct., Funct., Genet. 78*, 1950−1958.

(52) Wang, J. M., Wolf, R. M., Caldwell, J. W., Kollman, P. A., and Case, D. A. (2004) Development and testing of a general amber force field. *J. Comput. Chem. 25*, 1157−1174.

(53) Vriend, G. (1990) WHAT IF: a molecular modeling and drug design program. *J. Mol. Graphics 8*, 52−56.

(54) Dolinsky, T. J., Nielsen, J. E., McCammon, J. A., and Baker, N. A. (2004) PDB2PQR: an automated pipeline for the setup of Poisson-Boltzmann electrostatics calculations. *Nucleic Acids Res. 32*, W665−667.

(55) Darden, T., York, D., and Pedersen, L. (1993) Particle mesh Ewald: an N-log(N) method for Ewald sums in large systems. *J. Chem. Phys. 98*, 10089−10092.

(56) Miyamoto, S., and Kollman, P. A. (1992) SETTLE: An analytical version of the SHAKE and RATTLE algorithm for rigid water models. *J. Comput. Chem. 13*, 952−962.

(57) Bussi, G., Donadio, D., and Parrinello, M. (2007) Canonical sampling through velocity rescaling. *J. Chem. Phys. 126*, 014101.

(58) Parrinello, M., and Rahman, A. (1981) Polymorphic transitions in single crystals: A new molecular dynamics method. *J. Appl. Phys. 52*, 7182−7190.

(59) Hess, B., Bekker, H., Berendsen, H. J. C., and Fraaije, J. G. E. M. (1997) LINCS: A linear constraint solver for molecular simulations. *J. Comput. Chem. 18*, 1463−1472.

(60) Morra, G., Verkhivker, G., and Colombo, G. (2009) Modeling signal propagation mechanisms and ligand-based conformational dynamics of the Hsp90 molecular chaperone full-length dimer. *PLoS Comput. Biol. 5*, e1000323.

(61) Hu, Y.-J., Liu, Y., and Xiao, X.-H. (2009) Investigation of the interaction between berberine and human serum albumin. *Biomacromolecules 10*, 517−521.

(62) van de Weert, M. (2010) Fluorescence quenching to study protein-ligand binding: common errors. *J. Fluoresc. 20*, 625−629.